Met. Mater. Int., Vol. 22, No. 5 (2016), pp. 942~946
doi: 10.1007/s12540-016-6099-1

Crystallinity Dependent Gas-Sensing Abilities of ZnO Hollow Fibers

Akash Katoch, Zain Ul Abideen, Jae-Hun Kim, and Sang Sub Kim*

Department of Materials Science and Engineering, Inha University, Incheon 22212, Korea

(received date: 5 February 2016 / accepted date: 22 March 2016)

The grain size and crystallinity are important factors in considering the gas sensing properties of metal oxide based miniaturized gas sensors. This study reports the effects of the grain size and crystallinity on the CO sensing abilities of ZnO hollow fibers (HFs) synthesized by electrospinning. The grain size and crystallinity of the HFs were controlled by changing the heat treatment time during their synthesis and were characterized by SEM, TEM and XRD. Both the nanograin size and crystallinity of the HFs change significantly with increasing heat treatment time. Longer heat treatments result in improved sensing abilities irrespective of the evolution of larger-sized nanograins. Sensing measurements were carried out at various temperatures in the range 300-400 °C. The improved crystallinity likely compensates the adverse effects of grain growth in terms of the sensor response. That is, crystallinity rather than grain size, is the dominant factor determining the sensing abilities of HFs. This result provides useful guidelines for the fabrication of HF-based chemiresistive-type gas sensors.

Keywords: ZnO, hollow fiber, crystallinity, grain size, gas sensor

1. INTRODUCTION

In the field of gas sensing, metal-oxide nanofibers have attracted considerable interest because of their potential use in the detection of extremely low concentrations of toxic gases [1-5]. In particular, hollow fibers (HFs) have received more attention, not only because of their larger surface-to-volume ratios compared to regular solid fibers, but also because of their unique microstructural features, such as a cylindrical-fiber shape with an internal hollow space, which are mainly responsible for their physical and chemical properties [6-8].

The radial modulation of the electron-depleted layer established at both the outer and inner surface regions of n-type semiconducting oxide HFs was reported to be responsible for the resistance variations of the HFs during the adsorption/desorption of gas molecules [9]. More importantly, HFs were found to be efficient sensor materials for detecting reducing gases only, not oxidizing gases. Only a marginal increase in resistance will take place when an oxidizing gas is supplied to HFs because they are in the state of already-electron-depleted walls. When a reducing gas is supplied, the resistive wall of the HFs that is electron-depleted by the adsorption of oxygen species in air becomes less resistive due to the release of captured electrons back to the conduction band of the HFs. Therefore, the wall thickness of the HFs needs to be minimized to achieve the best sensor response for a reducing gas. In that report [9], the effects of the wall thickness of the ZnO HFs on their sensing properties were examined using CO as a representative reducing gas. The thin-walled HFs showed improved sensor responses to CO compared to the thick-walled HFs.

In addition, according to an earlier investigation and literature [10-12], the presence of more grain boundaries would likely hinder electronic transport, thereby suppressing electron mobility, which limits the applicability of the nanofibers in electronic devices where rapid electronic transport is a major concern. On the other hand, the presence of nanograins was found to be beneficial for gas-sensing applications [13-23]. The formation of a series of potential barriers at the grain boundaries is responsible for the more pronounced resistance variations of the nanofibers by gas molecules. Optimization of the size of nanograins was found to be essential for obtaining the maximal gas-sensing abilities, and the activation energy and growth mechanism of nanograins in oxide nanofibers have been investigated thoroughly [14,21-23].

In addition to the size of the nanograins, the crystallinity of nanofibers also greatly influences their gas-sensing properties [21,24,25]. To date, however, the effects of the size and crystallinity of the nanograins on the HFs is not known, and needs to be investigated to utilize HFs as chemiresistive-type gas sensors. In this study, ZnO HFs were synthesized by sequentially combining electrospinning and atomic layer deposition techniques (ALD), and their gas-sensing performance for a typical reducing gas CO was investigated as a function of the size and crystallinity of the nanograins. Crystallinity was found to play a dominant role in the gas-sensing properties of ZnO HFs.

*Corresponding author: sangsub@inha.ac.kr

These results provide useful guidelines for the fabrication of highly sensitive chemical sensors based on HFs.

2. EXPERIMENTAL PROCEDURES

ZnO HFs were synthesized using a process described in detail elsewhere [6,26]. The process included the following; (1) the synthesis of polymer fibers by electrospinning, (2) the subsequent deposition of ZnO layers by ALD, and (3) heat treatment to burn off the core polymer fibers. To avoid repetition, the precursors, electrospinning and ALD conditions are not described in this paper. The sacrificial polymer core was decomposed by heat treatment at 600 °C in air. Heat-treatment times, ranging from 0.5 to 18 h, were used to control the size and crystallinity of the nanograins in the ZnO HFs.

The phase and crystallinity of the ZnO HFs were examined by X-ray diffraction (XRD, Philips/X'pert MPD) using CuK_a radiation ($\lambda = 1.5418$Å). Their microstructure was examined by field-emission scanning electron microscopy (FE-SEM, Hitachi/S-4200) and transmission electron microscopy (HR-TEM, JEOL/JEM-2100F).

For the sensing measurements, 1×1 cm^2 SiO_2 (200 nm thick)-grown Si (100) substrates were used. Ti (~50 nm in thickness) and Pt (~200 nm) bilayers were deposited by sputtering Ti and Pt targets onto ZnO HFs using a comb-shape metal mask. A patterned interdigital electrode (IDE) consisting 8 fingers, 7 mm in length, 0.5 mm in width and 150 μm in spacing, was used to deposit the Ti/Pt bilayer electrode. The prepared sensor was then interfaced with a computer via an electric source meter (Keithley 2400). Figure 1 presents a schematic diagram of sensor fabrication. Details of the electrode fabrication procedure are described elsewhere [10,15]. The sensing capabilities of the ZnO HFs were investigated using CO, a representative reducing gas. The sensing measurements were performed using a gas-dilution and testing system and details of the measurement conditions are described elsewhere [15]. The sensor response (R) was determined according to the following equation: $R = R_a/R_g$, where R_a and R_g are the resistances in the absence and presence of CO, respectively.

3. RESULTS AND DISCUSSION

The microstructure and grain size of the ZnO HFs heat-treated for various times were investigated by FE-SEM, and the results are shown in Figure 2a-e. The diameter of the HFs was similar, ~390 nm. The insets reveal the hollow nature of the fibers, which consists of nanograins. The nanograins tend to grow with increasing heat treatment time. Figure 2f shows the size of the nanograins estimated from the FE-SEM images. Grain growth is well understood based on the diffusion of

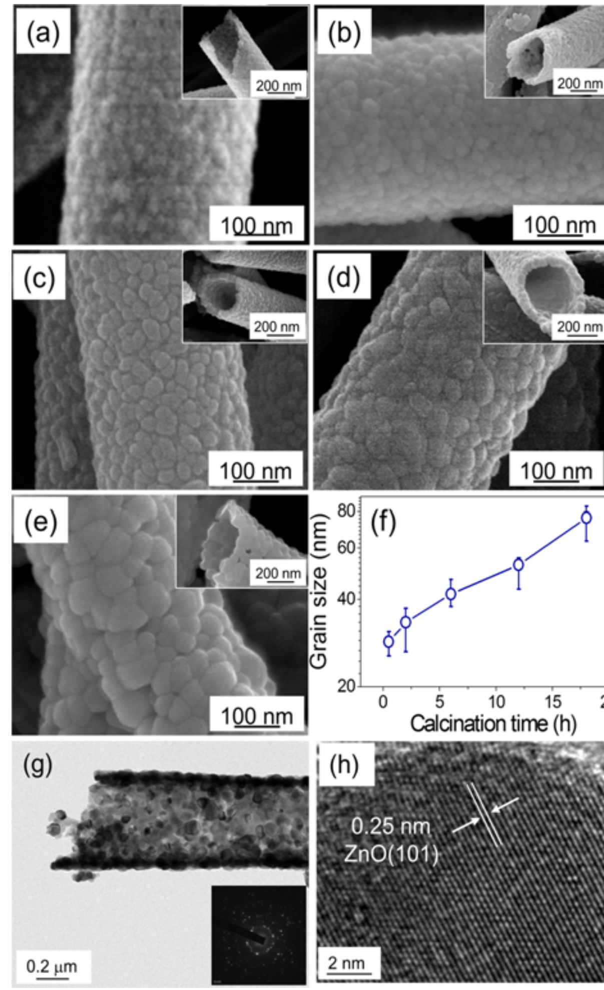

Fig. 2. FE-SEM images of ZnO HFs heat treated at 600 °C for various times; (a) 0.5, (b) 2, (c) 6, (d) 12, and (e) 18 h. (f) Change in the size of nanograins in ZnO HFs. (g) TEM image of a single ZnO HF heat treated for 12 h. The inset shows the SAED pattern of polycrystalline ZnO HFs. (h) High-resolution TEM image of a ZnO nanograin.

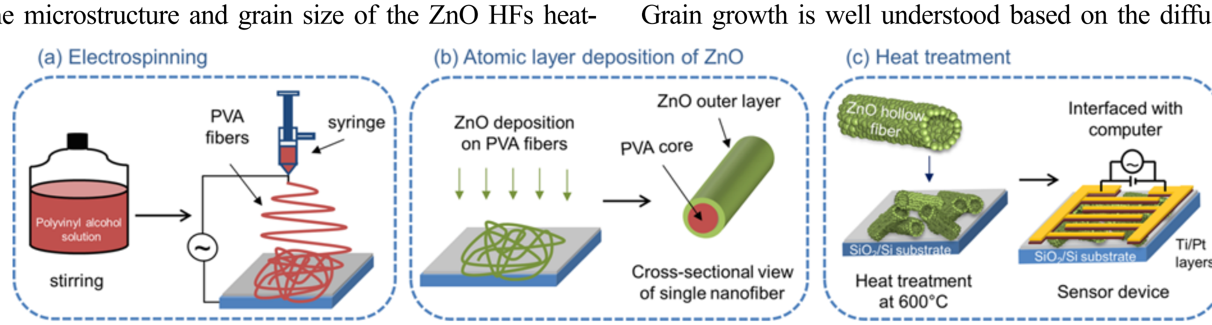

Fig. 1. Schematic diagram of the fabrication process of sensor devices using ZnO HFs.

atoms between adjacent grains. Atoms diffuse from the concave to the convex sides of the grain interfaces because of the higher chemical potential of atoms on the concave sides. The main driving force for growth of nanograins is the decrease in free energy of the system by lowering its grain boundary area [14,27,28]. Compared to the 0.5 h heat treatment, the size of the nanograins in the HFs increased by more than a factor of two when an 18 h heat treatment was used. This suggests that the growth of nanograins in HFs proceeds steadily, regardless of the restriction of HF walls, which are absent in regular, solid fibers.

The microstructure of the ZnO HFs was investigated further by TEM. Figure 2g presents a representative low-magnification TEM image taken from a single ZnO HF that had been heat-treated for 12 h. The light-grey core region with a black boarder suggests that the HF is hollow. The inset shows a selected area electron diffraction pattern, confirming the polycrystalline nature of the ZnO HF. Figure 2h shows a high-resolution TEM image of a ZnO nanograin. The clear lattice fringe with a spacing 0.25 nm is in good agreement with the (1 0 1) interplanar distance of the ZnO lattice.

The phase and crystallinity of ZnO HFs were determined by XRD. The results are shown in Fig. 3a. All the peaks match well with those of the hexagonal, wurtzite structured ZnO (JCPDS Card no. 891397), confirming the formation of a single ZnO phase. The XRD pattern taken from the as-electrospun ZnO fibers with a polymer core, which was produced by ALD without further heat treatment, is included for comparison. The integrated intensity of the XRD peaks is closely associated with the arrangement of atoms in the crystal planes. In this sense, the integrated intensity can be a yardstick used to qualitatively estimate the crystallinity of the ZnO fibers. The (1 0 1) XRD peak was chosen for that purpose because it was the most intense peak. Figure 3b shows the integrated intensities of the (1 0 1) XRD peaks as a function of the heat-treatment time. The inset presents a compilation of the (1 0 1) XRD peaks. It is reasonable to conclude that the crystallinity of the ZnO HFs was proportional to the heat-treatment time.

The CO-sensing capabilities of the ZnO HFs were investigated. Based on the results shown in Fig. S1 of the Supplementary Information, an optimal measurement temperature of 375 °C was used. The ZnO HFs heat-treated for 18 h, which had a mean grain size ~76.4 nm, were tested for CO sensing as a function of the operating temperature. Figure 4a presents a summary of the responses. As is evident from Fig. 4a, the best response to CO was obtained at 375 °C. Figure S2 of the Supplementary Information shows the resistance curves obtained from the ZnO HFs in the presence of 0.1, 1.0, 5.0, and 10.0 ppm CO. All the fabricated sensors clearly tracked the supply and stoppage of CO. This is typical behavior of an *n*-type semiconductor for reducing gases. Figure 4b summarizes the responses of the ZnO HFs, heat-treated for various times. For the purpose of showing the behavior of response as a function of calcination time more clearly, the response behavior of ZnO HFs for 0.1 ppm CO is summarized in Fig. 5a. As is evident, the sensor response increases with increasing the heat-treatment time.

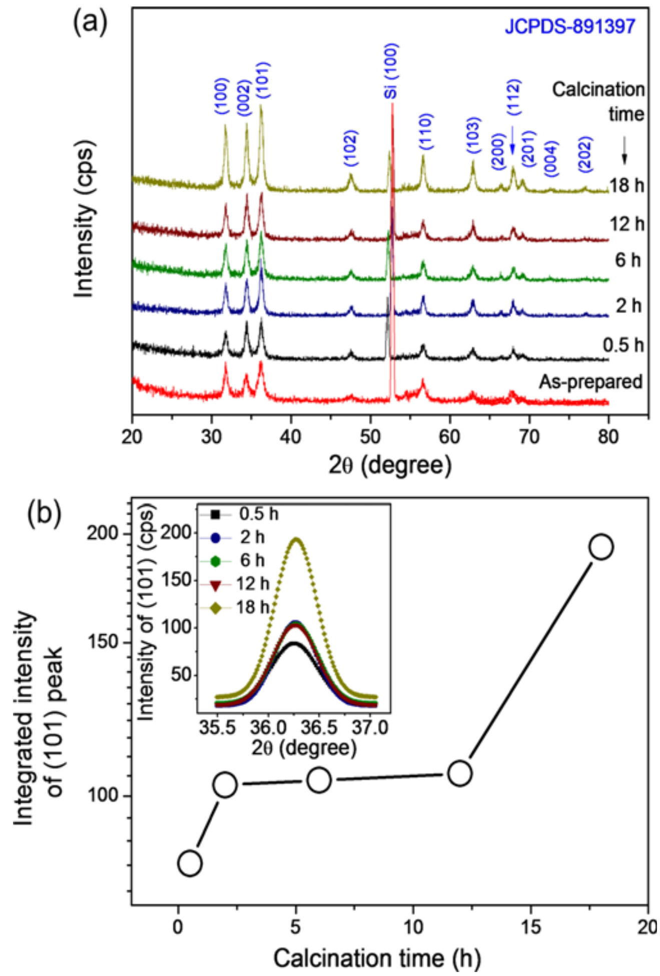

Fig. 3. XRD patterns of (a) ZnO HFs heat treated at 600 °C for various times. The XRD pattern of the as-electrospun ZnO fibers is included for comparison. (b) The integrated intensities of the (1 0 1) XRD peaks, as a function of the heat-treatment time. The inset presents a compilation of the (1 0 1) XRD peaks.

A change in the potential barrier of the nanograin boundaries is responsible for the resistance variation in the HFs during gas adsorption/desorption. Therefore, HFs with smaller grains will have stronger CO responses than the HFs with larger grains because smaller grains result in more grain boundaries; hence, more resistance variations. Therefore, HFs with smaller grains are supposed to have better sensing properties [28]. In contrast to this general expectation, ZnO HFs with smaller grains showed an inferior response than the HFs with larger grains. This suggests that there is another dominant factor determining the sensing properties of the ZnO HFs.

Similar to the case of normal, regular nanofibers [24,25,29], the crystallinity can be another important factor that can influ-

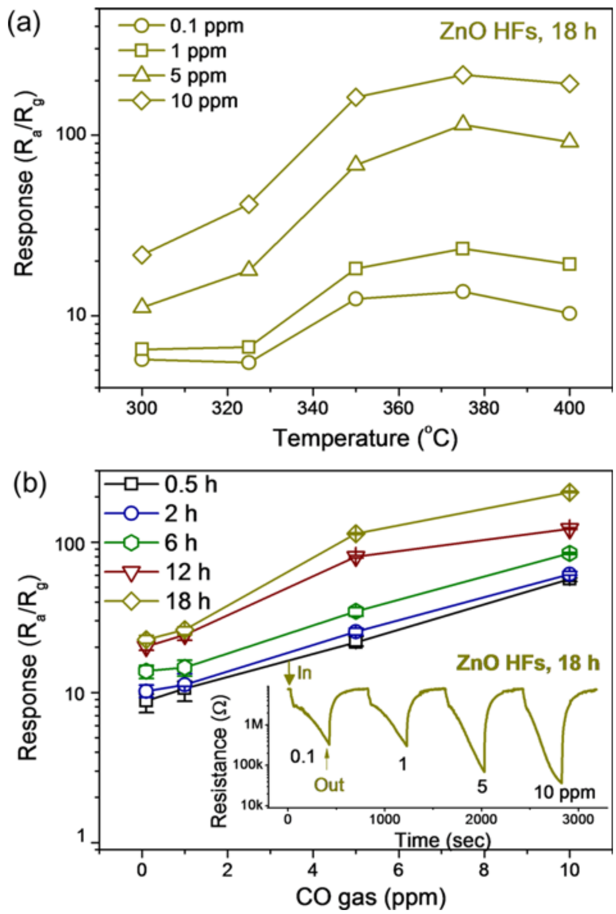

Fig. 4. Summarized responses of the ZnO HFs to the presence of CO gas; (a) heat treated for 18 h and tested as a function of temperature, ranging from 300 to 400 °C, and (b) heat treated for various times, ranging from 0.5 to 18 h, at 375 °C. The inset shows the dynamic resistance curve of ZnO HFs heat treated for 18 h.

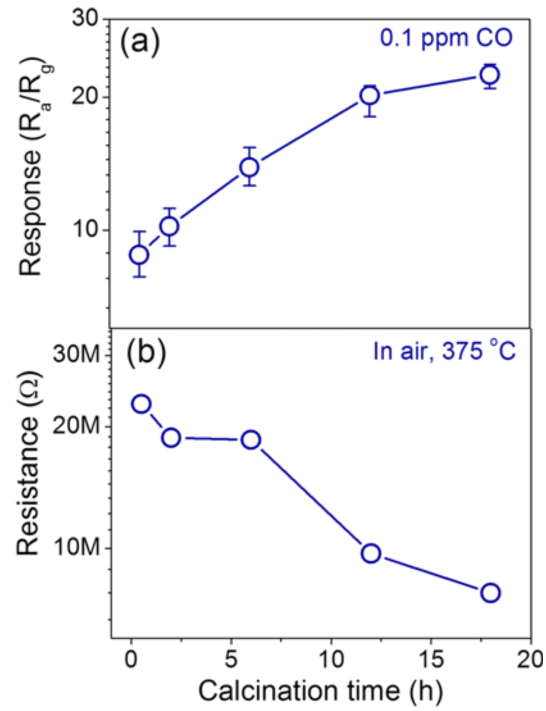

Fig. 5. Summary of (a) response of ZnO HFs to 0.1 ppm CO as a function of the heat-treatment time at 375 °C and (b) resistance in air at 375 °C.

ence gas-sensing properties of nanofibers. In general, grain imperfections and defects are the main sources of conduction in HFs. Low crystalline nanograins with more structural defects will possess more charge carriers, namely electrons. Therefore, a smaller resistance variation occurs during interaction of gas molecules, resulting in an inferior sensor response. In contrast, prolonged heat treatment improves the phase stability and crystallinity of the nanograins by reducing the number of structural defects [25]. Accordingly, HFs with higher crystallinity will contain fewer charge carriers, resulting in more pronounced resistance variations. Accordingly, the low crystalline ZnO HFs with more structural defects should be more conductive than high crystalline ones. On the other hand, the resistance of the ZnO HFs decreased with increasing heat-treatment time, as shown in Fig. 5b. It is of note that the overall resistance of the ZnO HFs is also influenced by the number of grain boundaries as well.

According to the current authors' earlier investigations on the electrical properties of ZnO nanofibers [10], they have about two orders of magnitude higher charge carrier concentration (1.3×10^{19} cm^{-3}), than the case of ZnO nanowires (7.5×10^{18} cm^{-3}). In contrast, the electron mobility in ZnO nanofibers (4.6×10^{-3} cm^2/Vs) is much lower by five orders of magnitude than ZnO nanowires (25.1 cm^2/Vs). In nanowires, the absence of grain boundaries and lesser point defects are responsible for the high mobility and lower charge carrier concentration in comparison to nanofibers. Based on this, the higher the crystalline quality is, the less the structural defects such as grain boundaries and point defects exist, and thus the lower the charge carrier concentration is. In ref. 24, the effect of grain size and crystallinity on the gas sensing performances of ZnO nanofibers was scrutinized by applying different calcination temperatures. It was found that in addition to the size, the crystallinity of the grains influences greatly the sensing performances. Two domains existed; (1) the crystallinity dominant domain and (2) the grain size dominant domain. Particularly, in the crystallinity-dominant domain, the enhancement of crystallinity overcame the adverse effect of grain growth, playing a dominant role in determining the sensing performances. The same scenario can be applied to ZnO HFs. However, because the sensor resistance depends both on the grain interior resistance and the grain boundary resistance, the measurement of the complex impedance spectra to deconvolute the resistances needs to be carried out at a next stage of research work.

In addition, the change of effective grain-boundary area in Hfs with different grain sizes obtained by heat treatment for different time can be another possible reason for the conduction change in Hfs. According to the earlier studies [30, 31], the effective contact area between the adjacent nanoparticles was found as one of the important parameters to determine the sensing ability of the metal oxide gas sensors. The increase in heat treatment time will enhance both grain size and contact area between grains. Considering the transducer function of gas sensor, the increase of chemiresistive contact area can positively contribute to the enhancement of sensor response. Meanwhile, the sensing properties of the sensor fabricated in this study were stable and reproducible for more than six months. An earlier investigation of the selectivity of ZnO HFs [9] revealed selectivity to CO gas over other gases, such as H_2, benzene and toluene.

4. CONCLUSIONS

Chemical sensors based on ZnO HFs were fabricated. HFs were synthesized by depositing ZnO layers onto electrospun sacrificial polymer fibers that were later removed by heat treatment. The size and crystallinity of the nanograins in the HFs were altered by varying the heat-treatment time. The size of the nanograins and the degree of crystallinity increased with increasing heat-treatment time. Interestingly, the CO-sensing properties of the ZnO HFs improved with increasing heat-treatment time. Considering that larger grains are detrimental to the gas-sensing abilities of nanofibers, it is evident that the crystallinity is more influential in determining the sensing properties of HFs than the grain size.

ACKNOWLEDGEMENTS

This work was supported by INHA UNIVERSITY Research Grant.

Electronic Supplemental Materials: The online version of this article(doi: 10.1007/s12540-016-6099-1) contains supplemental materials.

REFERENCES

1. S. Ramakrishna, K. Fujihara, W.E. Teo, T. Yong, Z.W. Ma, and R. Ramaseshan, *Mater. Today* **9**, 40 (2006).
2. O. Landau, A. Rothschild, and E. Zussman, *Chem. Mater.* **21**, 9 (2009).
3. E. Comini, C. Baratto, G. Faglia, M. Ferroni, A. Vomiero, and G. Sberveglieri, *Prog. Mater. Sci*. **54**, 1 (2009).
4. B. Ding, M. Wang, J. Yu, and G. Sun, *Sensors* **9**, 1609 (2009).
5. I. D. Kim, A. Rothschild, B. H. Lee, D. Y. Kim, S. M. Jo, and H. L. Tuller, *Nano Lett*. **6**, 2009 (2006).
6. A. Katoch, J. H. Kim, and S. S. Kim, *ACS Appl. Mater. Interfaces*. **6**, 21494 (2014).
7. S. W. Choi, J. Y. Park, C. Lee, J. G. Lee, and S. S. Kim, *J. Am. Ceram. Soc*. **94**, 1974 (2011).
8. S. H. Choi, G. Ankonina, D. Y. Youn, S. G. Oh, J. M. Hong, A. Rothschild, and *et al*., *ACS Nano* **3**, 2623 (2009).
9. A. Katoch, S. W. Choi, and S. S. Kim, *Nanotechnology* **25**, 455504 (2014).
10. J. Y. Park, J. J. Kim, and S. S. Kim, *Microelectron. Eng*. **101**, 8 (2013).
11. A. Kumar, R. Jose, K. Fujihara, J. Wang, and S. Ramakrishna, *Chem. Mater.* **19**, 6536 (2007).
12. J. Maier, *Nat. Mater*. **4**, 805 (2005).
13. A. Katoch, S. W. Choi, J. H. Kim, J. H. Lee, J. S. Lee, and S. S. Kim, *Sens. Actuators B* **214**, 111 (2015).
14. J. Y. Park, K. Asokan, S. W. Choi, and S. S. Kim, *Sens. Actuators B* **152**, 254 (2011).
15. S. W. Choi, J. Y. Park, and S. S. Kim, *Chem. Eng. J.* **172**, 550 (2011).
16. G.-Y. Cha, A.-H. Bui, W.-W. Baek, S.-T. Lee, D.-D. Lee, and J.-S. Huh, *Met. Mater. Int*. **10**, 149 (2004).
17. R. Viter, A. Katoch, and S. S. Kim, *Met. Mater. Int*. **20**, 163 (2014).
18. A. Katoch, S.-W. Choi, G.-J. Sun, H. W. Kim, and S. S. Kim, *J. Hazard. Mater.* **286** 229 (2015).
19. A. Katoch, S.-W. Choi, J.-H. Kim, J. H. Lee, J.-S. Lee, and S. S. Kim, *Sens. Actuators B* **214**, 111 (2015).
20. A. Katoch, Z. U. Abideen, H. W. Kim, and S. S. Kim, *ACS Appl. Mater. Interfaces* **8**, 2486 (2016).
21. S. W. Choi, J. Y. Park, and S. S. Kim, *J. Mater. Res*. **26**, 1662 (2011).
22. J. Y. Park, S. W. Choi, K. Asokan, and S. S. Kim, *Met. Mater. Int*. **16**, 785 (2010).
23. J. Y. Park and S. S. Kim, *J. Am. Ceram. Soc*. **92**, 1691 (2009).
24. A. Katoch, G. J. Sun, S. W. Choi, J. H. Byun, and S. S. Kim, *Sens. Actuators B* **185**, 411 (2013).
25. T. Senthil and S. Anandhan, *J. Colloid Interf. Sci*. **432**, 285 (2014).
26. J. Y. Park, S. W. Choi, and S. S. Kim, *Nanotechnology* **21**, 475601 (2010).
27. A. Katoch, S. W. Choi, and S. S. Kim, *Met. Mater. Int*. **21**, 213 (2015).
28. N. Barsan and U. Weimar, *J. Electroceram*. **7**, 143 (2001).
29. X. Q. Pan, L. Fu, and J. E. Dominguez, *J. Appl. Phys*. **89**, 6056 (2001).
30. J.-W. Yoon, J.-K. Choi, and J.-H. Lee, *Sens. Actuators B* **161**, 570 (2012).
31. X. Wan, J. Wang, and L. Zhu, J. Tang, *J. Mater. Chem. A* **2**, 13641 (2014).